Pharm Res (2019) 36: 18
https://doi.org/10.1007/s11095-018-2548-5

RESEARCH PAPER

Different Efflux Transporter Affinity and Metabolism of ^{99m}Tc-2-Methoxyisobutylisonitrile and ^{99m}Tc-Tetrofosmin for Multidrug Resistance Monitoring in Cancer

Masato Kobayashi[1] • Takafumi Tsujiuchi[2] • Yuya Okui[2] • Asuka Mizutani[2] • Kodai Nishi[3] • Takeo Nakanishi[4] • Ryuichi Nishii[5] • Kazuki Fukuchi[6] • Ikumi Tamai[4] • Keiichi Kawai[2,7]

Received: 2 September 2018 / Accepted: 21 November 2018 / Published online: 29 November 2018

ABSTRACT

Background Little is known about the affinity and stability of ^{99m}Tc-labeled 2-methoxyisobutylisonitrile (^{99m}Tc-MIBI) and tetrofosmin (^{99m}Tc-TF) for imaging of multiple drug resistance transporters in cancer. We examined the affinity of ^{99m}Tc-labeled compounds for these transporters and their stability.

Methods ^{99m}Tc-MIBI and ^{99m}Tc-TF were incubated in vesicles expressing P-glycoprotein (MDR1), multidrug resistance-associated protein (MRP)1–4, or breast cancer resistance protein with and without verapamil (MDR1 inhibitor) or MK-571 (MRP inhibitor). Time activity curves of ^{99m}Tc-labeled compounds were established using SK-N-SH neuroblastoma, SK-MEL-28 melanoma, and PC-3 prostate adenocarcinoma cell lines, and transporter expression of multiple drug resistance was measured in these cells. The stability was evaluated.

Results In vesicles, ^{99m}Tc-labeled compounds had affinity for MDR1 and MRP1. ^{99m}Tc-TF had additional affinity for MRP2 and MRP3. In SK-N-SH cells expressing MDR1 and MRP1, MK-571 produced the highest uptake of both ^{99m}Tc-labeled compounds. ^{99m}Tc-MIBI uptake with inhibitors was higher than ^{99m}Tc-TF uptake with inhibitors. ^{99m}Tc-TF was taken up more in SK-MEL-28 cells expressing MRP1 and MRP2 than PC-3 cells expressing MRP1 and MRP3. ^{99m}Tc-MIBI was metabolized, whereas ^{99m}Tc-TF had high stability.

Conclusion ^{99m}Tc-MIBI is exported via MDR1 and MRP1 (MRP1 > MDR1) at greater levels and more quickly compared to ^{99m}Tc-TF, which is exported via MDR1 and MRP1–3 (MRP1 > MDR1; MRP1, 2 > MRP3). Because ^{99m}Tc-MIBI is metabolized, clinical imaging for monitoring MDR and shorter examination times may be possible with an earlier scanning time on late phase imaging. ^{99m}Tc-TF has high stability and accurately reflects the function of MDR1 and MRP1–3.

KEY WORDS ^{99m}Tc-MIBI · ^{99m}Tc-tetrofosmin · adenosine triphosphate-binding cassette transporters · multidrug resistance · multidrug resistance-associated protein

✉ Masato Kobayashi
kobayasi@mhs.mp.kanazawa-u.ac.jp

1 Wellness Promotion Science Center, Institute of Medical, Pharmaceutical and Health Sciences Kanazawa University
5-11-80 Kodatsuno, Kanazawa 920-0942, Japan

2 School of Health Sciences, Institute of Medical, Pharmaceutical and Health Sciences Kanazawa University
Kanazawa, Japan

3 Department of Radioisotope Medicine
Atomic Bomb Disease Institute Nagasaki University
Nagasaki, Japan

4 School of Pharmaceutical Sciences, Institute of Medical, Pharmaceutical and Health Sciences Kanazawa University
Kanazawa, Japan

5 Department of Molecular Imaging and Theranostics
National Institute of Radiological Sciences
Chiba, Japan

6 Graduate School of Medicine, Division of Health Sciences
Osaka University
Osaka, Japan

7 Biomedical Imaging Research Center University of Fukui
Fukui, Japan

INTRODUCTION

Multiple drug resistance (MDR) in cancer is often associated with an adenosine triphosphate (ATP)-dependent decrease in cellular drug accumulation and is attributed to the overexpression of certain ATP-binding cassette (ABC) transporter proteins. ABC transporters belong to the largest transporter gene family and generally use energy derived from ATP hydrolysis for translocation of different substrates across biological membranes. ABC transporters are classified into seven subfamilies based on phylogenetic analysis and are designated ABCA to ABCG (1). In tumor cell lines, ABC proteins mainly

include P-glycoprotein (MDR1) (gene symbol *ABCB1*), the multidrug resistance protein 1 (MRP1, gene symbol *ABCC1*), MRP2 (gene symbol *ABCC2*), MRP3 (gene symbol *ABCC3*), MRP4 (gene symbol *ABCC4*), and breast cancer resistance protein (BCRP, gene symbol *ABCG2*).

^{99m}Tc-labeled 2-methoxyisobutylisonitrile (^{99m}Tc-MIBI) and ^{99m}Tc-labeled tetrofosmin (^{99m}Tc-TF) are lipophilic monocationic radiotracers that are widely used for myocardial perfusion imaging (2) and tumor imaging (3) in single photon emission computed tomography (SPECT) studies. In tumor imaging, MDR to anticancer drugs has been estimated using both ^{99m}Tc-labeled compounds in clinical studies (4,5). ABC transporters, which are associated with MDR, are often highly expressed in cancer cells. ^{99m}Tc-labeled compounds are mainly exported via MDR1 (6–8) and MRP1 (7). Many ABC transporters, not only MDR1 and MRP1 but also MRP2–4 (9–11) and BCRP (12), are expressed in cancer cells. However, whether MRP2–4 and BCRP are associated with export of ^{99m}Tc-labeled compounds has not been clearly determined.

If ^{99m}Tc-labeled compounds are metabolized completely and immediately after injection *in vivo*, monitoring of MDR in cancers may be affected in clinical SPECT imaging because metabolites of ^{99m}Tc-labeled compounds may not be taken up in cancers and undergo efflux through MDR when clinical imaging is performed in the early phase (10–30 min) and the late phase (2–3 h) after injection (4,5). However, the stability of ^{99m}Tc-labeled compounds has not been sufficiently evaluated *in vivo*. We examined whether ^{99m}Tc-labeled compounds were exported via MRP2–4 and BCRP and whether these compounds had affinity for these transporters including MDR1 and MRP1 in cancer cells. Furthermore, stability of the ^{99m}Tc-labeled compounds over time was investigated in a human-derived cancer cell line, mouse liver, and human liver, which is an important organ for metabolism.

MATERIALS AND METHODS

Materials

^{99m}Tc-MIBI (300 MBq/mL) and ^{99m}Tc-TF (592 MBq/mL) injection kits were purchased from FUJIFILM RI Pharma Co., Ltd. (Chiba, Japan) and Nihon Medi-physics Co., Ltd. (Chiba, Japan), respectively. $^{99m}TcO_4^-$ was eluted from a ^{99}Mo/^{99m}Tc-column generators (Nihon Medi-physics Co., Ltd., Chiba, Japan). β-nicotinamide-adenine dinucleotide phosphate (β-$NADP^+$) and glucose-6-phosphate dehydrogenase were purchased from Oriental Yeast (Osaka, Japan). Verapamil hydrate and MK-571 sodium salt were purchased from Sigma-Aldrich (St. Louis, MO, USA) and Cayman Chemical (Ann Arbor, MI, USA), respectively. Human liver S9 was purchased from Corning Gentest (New York, NY, USA).

Vesicles

We used ABC transporter vesicles (GenoMembrane Inc., Kanagawa, Japan) transfected with human MDR1, MRP1–4, and BCRP. Experimental kits were also purchased from GenoMembrane Inc. and were used for experiments with each ABC transporter.

Vesicle Assay

After pre-incubation of vesicles for 10 min, 37 kBq ^{99m}Tc-labeled compound was incubated for 5 min with each vesicle solution and ATP, which supplies energy for ABC transporters, or adenosine monophosphate (AMP), which does not provide energy and was used for comparison to ATP, on nitrocellulose filters, and the radioactivity was measured using a γ-ray counter (AccuFLEXγ7000, Aloka, Tokyo, Japan) (13). Uptake of ^{99m}Tc-MIBI or ^{99m}Tc-TF in ATP solution was compared with that in AMP solution. When uptake of ^{99m}Tc-MIBI or ^{99m}Tc-TF in ATP solution was higher than that in AMP solution, this indicated an effect on ABC transporters for ^{99m}Tc-MIBI or ^{99m}Tc-TF. In assays with inhibitors, uptake of ^{99m}Tc-MIBI or ^{99m}Tc-TF was examined in ATP solution with verapamil, a MDR1 inhibitor, or MK-571, a MRP inhibitor.

Cancer Cells

The following cultured human cancer cell lines were purchased from American Type Culture Collection (Manassas, VA, USA): SK-N-SH neuroblastoma, SK-MEL-28 melanoma, and PC-3 prostate adenocarcinoma. Cancer cells were incubated in αMEM (Wako, Osaka, Japan; SK-N-SH cells) or Dulbecco's Modified Eagle's Medium (Wako; SK-MEL-28 cells) or RPMI-1640 Medium (Sigma; PC-3 cells) with 10% fetal bovine serum.

Expression of ABC Transporters in Human Cancer Cells

Expression of ABC transporters in human cancer cells was evaluated as described (14). The following genes were analyzed using real-time polymerase chain reaction with a Mx3005P thermocycler (Agilent Technologies, Santa Clara, CA, USA): MDR1 (*ABCB1*) and MRP1, 2, 3 (*ABCC1*, *2*, and *3*) as summarized in Table I. Three different housekeeping genes, glyceraldehyde-3-phosphate dehydrogenase (*GAPDH*), beta actin (*ACTB*), and hypoxanthine phosphoribosyltransferase-1 (*HPRT1*), were amplified to control for the differences between the initial RNA and cDNA amounts.

Table I Expression of Genes Encoding the ABC Transporters in Human Cancer Cells

Transporter	Gene symbol	SK-N-SH	SK-MEL-28	PC-3
MDR1	*ABCB1*	25.83	0.02	0.00
MRP1	*ABCC1*	23.41	7.81	20.60
MRP2	*ABCC2*	0.16	11.61	0.26
MRP3	*ABCC3*	0.75	0.00	21.39

Data are expressed as copy number per 1000 copies of housekeeping genes

Assay with Human Cancer Cells

Transport assays were performed as described (13). One day after seeding of cancer cells, each well was pre-incubated with 1 mL incubation medium for 10 min. The cells were then incubated with 37 kBq ^{99m}Tc-MIBI or ^{99m}Tc-TF for 5, 10, 30, or 60 min at 37°C.

For the competitive inhibition assay, the cells were incubated for 5 min with ^{99m}Tc-MIBI or ^{99m}Tc-TF in the presence of inhibitor: final concentration 50 μM verapamil hydrate for MDR1 (15) or 50 μM MK-571 sodium salt for MRP1–4 (16). At the end of the incubation, each well was rapidly washed twice with 1 mL ice-cold incubation medium. The cells were then solubilized in 0.5 mL 0.1 N NaOH, and radioactivity was measured with a γ-ray counter.

SPECT Imaging of ^{99m}Tc-Labeled Compounds in SK-N-SH-Bearing Mice

All animal studies were conducted following approval by the Animal Care Committee of Kanazawa University (AP-122339). Five Scid mice (female, 5 weeks old) were transplanted with SK-N-SH cells (5×10^5 cells/100 μL) and Matrigel (#354230, Corning, NY, USA) into the lower abdomen of the mice. The mice were housed for about 5–7 weeks under a 12-h light/12-h dark cycle with free access to food and water. Each ^{99m}Tc-labeled compound (20–30 MBq) was injected into the tail vein of cancer-bearing mice, and SPECT acquisition was started 5 min after injection and continued for 90 min every 5 min using a U-SPECT-II/CT system (MILabs, Utrecht, The Netherlands). The data were reconstructed using the ordered subset expectation maximization method with 16 subsets and six iterations including no scatter and attenuation correction. The voxel size was set to $0.8 \times 0.8 \times 0.8$ mm. Post-reconstruction smoothing filtering was applied using a 1.0-mm Gaussian filter. Image displays were obtained using medical image data analysis software, AMIDE (ver. 1.0.2). Coronal images were displayed as maximum intensity projections. In these images, three to five regions of interest were placed over the parathyroid, heart, liver, gallbladder, and kidney, and the time activity curve of each was obtained.

Time Stability of ^{99m}Tc-Labeled Compounds in SK-N-SH-Bearing Mice and Human Liver S9

Three mice each (total 15 mice) were killed at 5, 10, 20, 30, and 60 min after injection of 185 MBq ^{99m}Tc-labeled compounds. After blood sampling via cardiocentesis, the SK-N-SH cells and mouse livers were removed. Metabolites in SK-N-SH cells, mouse liver, and plasma were analyzed by thin layer chromatography (TLC). Human liver S9 was also used for metabolic analysis. Briefly, Krebs-Ringer phosphate buffer (pH 7.4) was added to the samples, followed by homogenization with an ultrasonic homogenizer (SONIFIER250, Branson, MO, USA). Then, ethanol was added to the homogenate to remove proteins, and the sample including blood was centrifuged for 5 min at 18,000×*g*. The final supernatant was spotted onto the TLC plate, and the TLC spots were developed using acetonitrile:methanol:0.5 mol/L ammonium acetate:tetrahydrofuran at a ratio of 4:3:2:1 for ^{99m}Tc-MIBI (17) and dichloromethane:acetone at a ratio of 13:7 for ^{99m}Tc-TF (17–19). The rates of flow (Rf) for ^{99m}Tc-MIBI and ^{99m}Tc-TF were in the ranges of 0.15–0.25 and 0.20–0.30, respectively. After development and complete drying, the TLC plates were cut into 20 fractions, and the radioactivity associated with each fraction was measured using a γ-ray counter. The fractional ratios of metabolites were calculated by dividing the radioactive counts for each fraction by the total radioactivity count.

Statistical Analysis

Data are presented as the means and standard deviation (SD). *P* values were calculated using the two-tailed paired Student's *t* test for comparison between two groups. A *P* value less than 0.05 was considered significant.

RESULTS

In the vesicle assay (Fig. 1), uptake of neither ^{99m}Tc-MIBI nor ^{99m}Tc-TF in ATP solution was significantly different from uptake in AMP solution in control vesicles. The uptake of ^{99m}Tc-MIBI was significantly different in ATP solution compared to AMP solution in MDR1 and MRP1 vesicles, whereas ^{99m}Tc-TF showed significantly higher uptake in not only vesicles expressing MDR1 and MRP1 but also vesicles expressing MRP2 and MRP3. Loading with verapamil for MDR1 or MK-571 for MRP restored the uptake to levels similar to that in AMP solution for both ^{99m}Tc-labeled compounds. Regarding the expression of ABC transporters in cancer cells (Table I), all cancer cells showed high MRP1 expression. In addition, we observed high expression of MDR1 in SK-N-SH cells, MRP2 in SK-MEL-28 cells, and MRP3 in PC-3 cells.

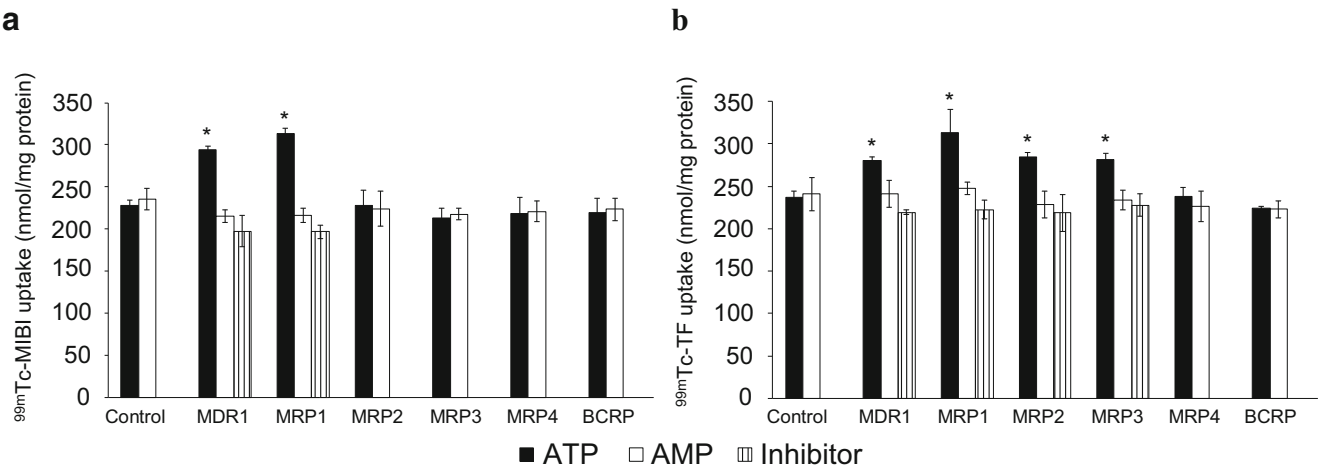

Fig. 1 Uptake of ^{99m}Tc-MIBI (**a**) and ^{99m}Tc-TF (**b**) after 5 min of incubation in vesicles that highly express each ABC transporter. For ^{99m}Tc-MIBI, uptake via MDR1 and MRP1 in ATP solution was significantly higher than uptake in AMP solution, and each inhibitor in ATP solution decreased the uptake to the level in AMP solution. For ^{99m}Tc-TF, uptake via MDR1, MRP1, MRP2, and MRP3 in ATP solution was significantly higher than uptake in AMP solution, and uptake was blocked by each inhibitor. *$P < 0.01$ between uptake in ATP and AMP solution ($n = 5$; paired t test).

In the time activity curves for ^{99m}Tc-MIBI and ^{99m}Tc-TF in SK-N-SH cells (Fig. 2), verapamil or MK-571 loading produced significantly higher uptake than in the control at all incubation times. At 5 min of incubation, uptake of ^{99m}Tc-MIBI and verapamil loading was 2.1-fold higher than in the control, and that with MK-571 loading was 2.8-fold higher (Fig. 2a). Uptake of ^{99m}Tc-TF and verapamil loading was 1.8-fold higher than the control condition, and that with MK-571 loading was 2.3-fold higher (Fig. 2b).

^{99m}Tc-MIBI with MK-571 loading produced higher accumulation than in the control condition in both SK-MEL-28 and PC-3 cells at all incubation times (Fig. 3a). Time activity curves of ^{99m}Tc-MIBI with MK-571 loading showed very little difference in accumulation in both cancer cell lines.

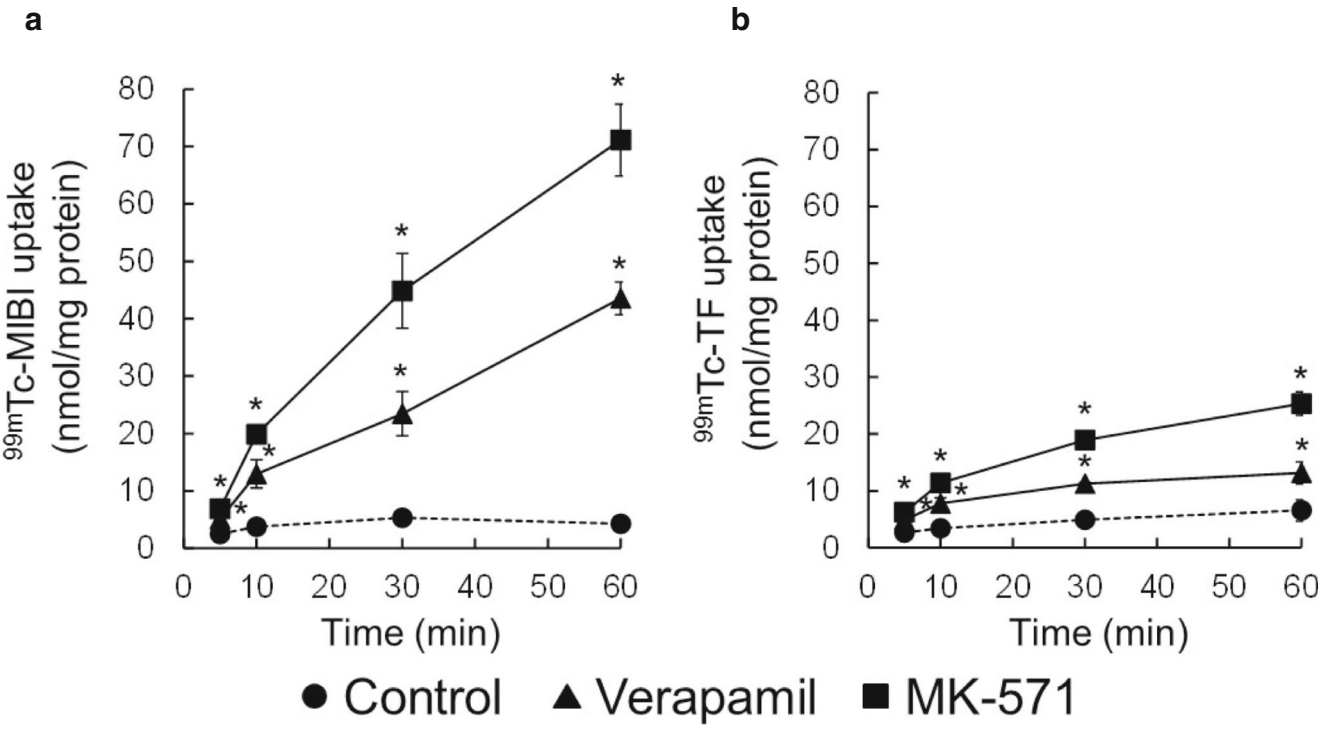

Fig. 2 Time activity curves for ^{99m}Tc-MIBI (**a**) and ^{99m}Tc-TF (**b**) in SK-N-SH cells, which highly expressed MDR1 and MRP1. For both ^{99m}Tc-labeled compounds, loading with MK-571, a MRP inhibitor, produced the highest uptake despite similar expression levels of MDR1 and MRP1. Time activity curves of ^{99m}Tc-MIBI with each inhibitor showed higher uptake than that of ^{99m}Tc-TF with each inhibitor. *$P < 0.01$ between uptake of ^{99m}Tc-labeled compounds and control ($n = 4$; paired t test).

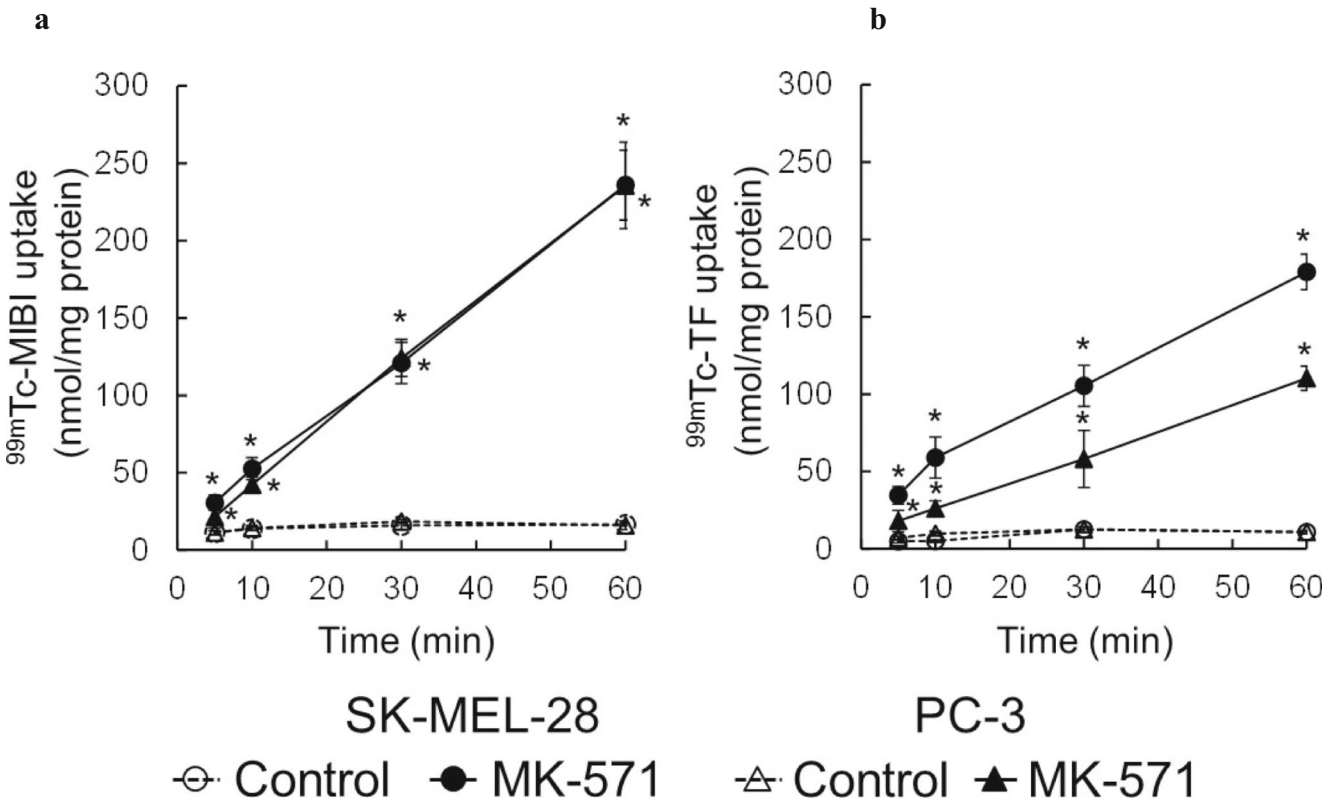

Fig. 3 Time activity curves of ^{99m}Tc-MIBI (**a**) and ^{99m}Tc-TF (**b**) in SK-MEL-28 and PC-3 cells. ^{99m}Tc-MIBI with MK-571 loading (●; SK-MEL-28 and ▲; MK-571) produced higher accumulation than the control condition (○; SK-MEL-28 and △; MK-571) in both cell lines at all incubation times. Time activity curves of ^{99m}Tc-MIBI with MK-571 loading showed very little difference in accumulation in both cancer cell lines. Time activity curves of ^{99m}Tc-TF with MK-571 loading in SK-MEL-28 cells, which expressed MRP1 and MRP2, showed higher uptake than that in the control condition and PC-3 cells, which expressed MRP1 and MRP3. *$P < 0.01$ between the uptake of ^{99m}Tc-labeled compounds in SK-MEL-28 and PC-3 cells compared to the control condition (n = 4; paired *t* test).

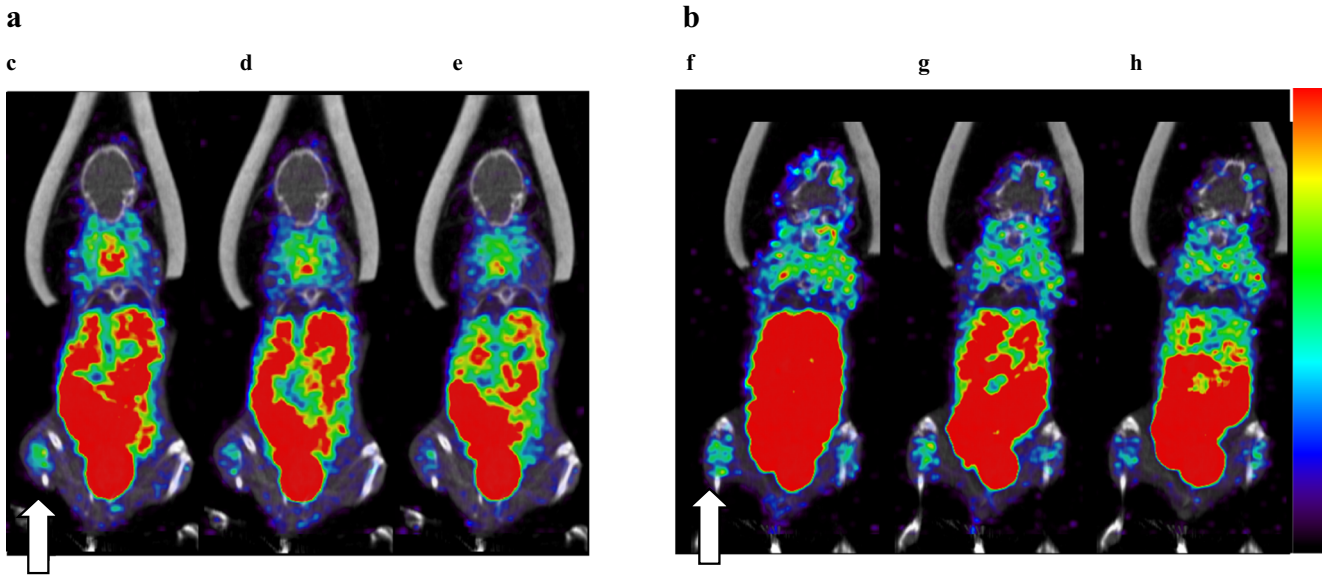

Fig. 4 Whole-body images of SK-N-SH-bearing mice under 2.0% isoflurane anesthesia injected with 20–30 MBq ^{99m}Tc-MIBI (**A**) or ^{99m}Tc-TF (**B**) at 5–10 min (c, f), 30–35 min (d, g), and 55–60 min (e, h). The arrows show solid cancers of SK-N-SH cells. The accumulation between brain and lung was in brown adipocytes around the neck. Although accumulation in SK-N-SH cells was lower than in abdominal organs at all acquisition times, similar accumulation levels were seen between ^{99m}Tc-MIBI (c) and ^{99m}Tc-TF (f) at 5–10 min after injection. At 30–35 min, we observed that the accumulation of ^{99m}Tc-MIBI was lower than that of ^{99m}Tc-TF. Background levels of ^{99m}Tc-TF were higher than those of ^{99m}Tc-MIBI. Time activity curves were obtained for the whole body (Fig. 5) and SK-N-SH cells (Fig. 6).

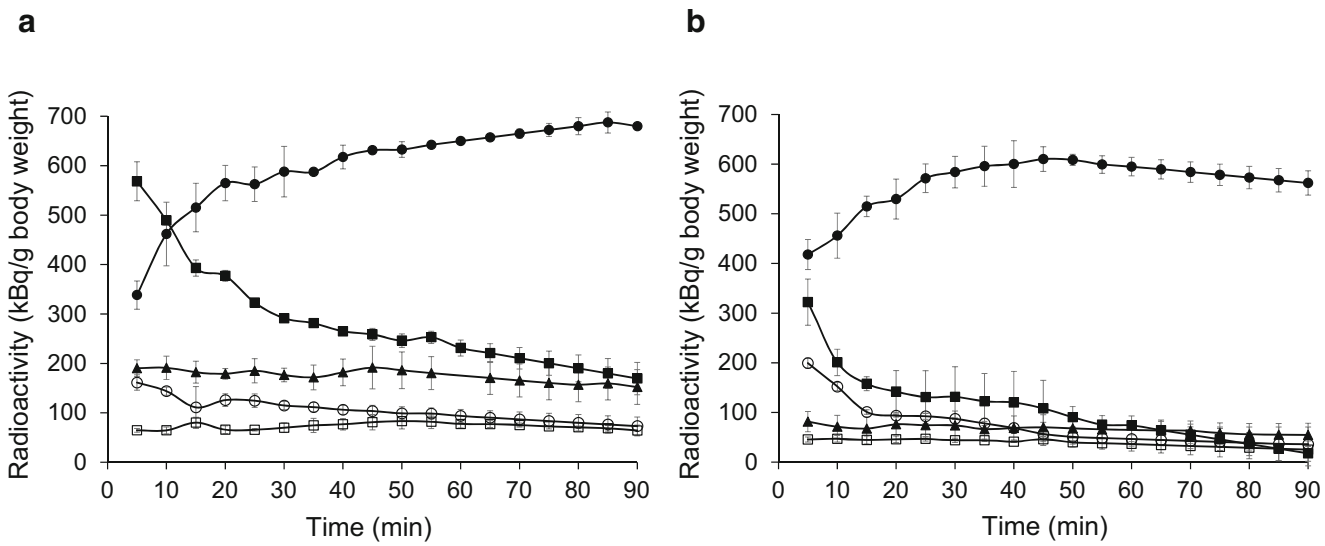

Fig. 5 Time activity curves of each organ obtained from 5-min acquisition images in SK-N-SH-bearing mice injected with 20–30 MBq ^{99m}Tc-MIBI (**a**) or ^{99m}Tc-TF (**B**). In the gallbladder (●), accumulation was higher than in other organs, whereas faster excretion was found in kidney (■). In liver (○), ^{99m}Tc-TF showed higher accumulation than ^{99m}Tc-MIBI at 10 min after injection. In the parathyroid (▲) and heart (□), accumulation did not change much over time, but ^{99m}Tc-MIBI showed higher accumulation than ^{99m}Tc-TF. The error bars show standard deviation of data from five mice

Time activity curves of ^{99m}Tc-TF with MK-571 loading in SK-MEL-28 cells showed the highest uptake (Fig. 3b).

Whole-body images of SK-N-SH-bearing mice were obtained for ^{99m}Tc-MIBI (Fig. 4a) and ^{99m}Tc-TF (Fig. 4b) at 5–10 min (c, f), 30–35 min (d, g), and 55–60 min (e, h). The accumulation between brain and lung was in brown adipocytes around the neck. Accumulation in SK-N-SH cells was lower than in abdominal organs at all acquisition times. Although we observed similar accumulation levels in SK-N-SH cells between ^{99m}Tc-MIBI (Fig. 4Ac) and ^{99m}Tc-TF (Fig. 4Bf) at 5–10 min after injection, accumulation of ^{99m}Tc-MIBI in liver was lower than that of ^{99m}Tc-TF. At 30–35 min, we observed that the accumulation of ^{99m}Tc-MIBI in SK-N-SH cells was lower than that of ^{99m}Tc-TF. Background levels of ^{99m}Tc-MIBI were also lower than those of ^{99m}Tc-TF.

The whole-body distributions of ^{99m}Tc-MIBI (Fig. 5a) and ^{99m}Tc-TF (Fig. 5b) were obtained from whole-body images. Accumulation in the gallbladder was higher than that in other organs, and excretion via the kidneys was fast. In liver, ^{99m}Tc-TF had higher accumulation than ^{99m}Tc-MIBI at 10 min after injection as shown in Fig. 4. In the parathyroid and heart, these accumulations did not change much over time, but ^{99m}Tc-MIBI accumulated more than ^{99m}Tc-TF.

Time activity curves of SK-N-SH cells (Fig. 6) from whole-body images in Fig. 4 showed that more ^{99m}Tc-MIBI underwent significant efflux from the tumors than ^{99m}Tc-TF during the first 50 min after injection. ^{99m}Tc-MIBI underwent rapid efflux from the tumors until about 30 min after injection, and then showed moderate efflux, whereas ^{99m}Tc-TF underwent gradual efflux from the tumors over time (Fig. 6a). Regarding accumulation in SK-N-SH cells of ^{99m}Tc-MIBI (Fig. 6b) and ^{99m}Tc-TF (Fig. 6c) with verapamil or MK-571 loading, MK-571 loading yielded higher accumulation with the two ^{99m}Tc-labeled compounds because MRP in SK-N-SH cells was inhibited by MK-571. In the time activity curves of ^{99m}Tc-MIBI (Fig. 6b), both inhibitors provided significantly higher accumulation than the control condition at about 30 min after injection. In the time activity curves of ^{99m}Tc-TF (Fig. 6c), verapamil loading led to an increase in accumulation at about 10 min, whereas MK-571 loading led to an increase in accumulation at about 50 min.

Regarding the stability over time for both ^{99m}Tc-labeled compounds in SK-N-SH cells, mouse liver, plasma, and human liver S9 fractions (Table II), the Rf values of ^{99m}Tc-MIBI, ^{99m}Tc-TF, and $^{99m}TcO_4^-$ were in the ranges of 0.15–0.25, 0.20–0.30, and 0.85–0.95 in our study, respectively. Although both ^{99m}Tc-labeled compounds were slightly metabolized up to 20 min after injection in all tissues, the radiochemical fraction of ^{99m}Tc-MIBI shifted from 97.5 ± 3.2% to 32.4 ± 17.5%, 26.3 ± 14.2%, 79.9 ± 18.5%, and 62.9 ± 12.1% in SK-N-SH cells, mouse liver, human liver S9 fractions, and

Fig. 6 Time activity curves of SK-N-SH cells obtained from 5-min acquisition images in SK-N-SH-bearing mice injected with 20–30 MBq ^{99m}Tc-MIBI or ^{99m}Tc-TF. In the control condition (**a**), more ^{99m}Tc-MIBI (○) underwent efflux from the tumors than ^{99m}Tc-TF (□) during the first 50 min after injection. ^{99m}Tc-MIBI underwent rapid efflux from the tumors until about 30 min after injection and then underwent moderate efflux, whereas ^{99m}Tc-TF underwent gradual efflux from the tumors over time. For both ^{99m}Tc-labeled compounds with inhibitors, MK-571 loading (● or ■ solid line) for MRP inhibition yielded the highest accumulation. ^{99m}Tc-MIBI (**b**) with verapamil loading (● and dotted line) and MK-571 loading (● and solid line) accumulated at significantly higher levels than in the control condition during the first ~30 min. ^{99m}Tc-TF (**c**) with verapamil loading (■ and dotted line) showed increased accumulation during the first 10 min, whereas MK-571 loading (■ and solid line) increased the accumulation during the first 50 min

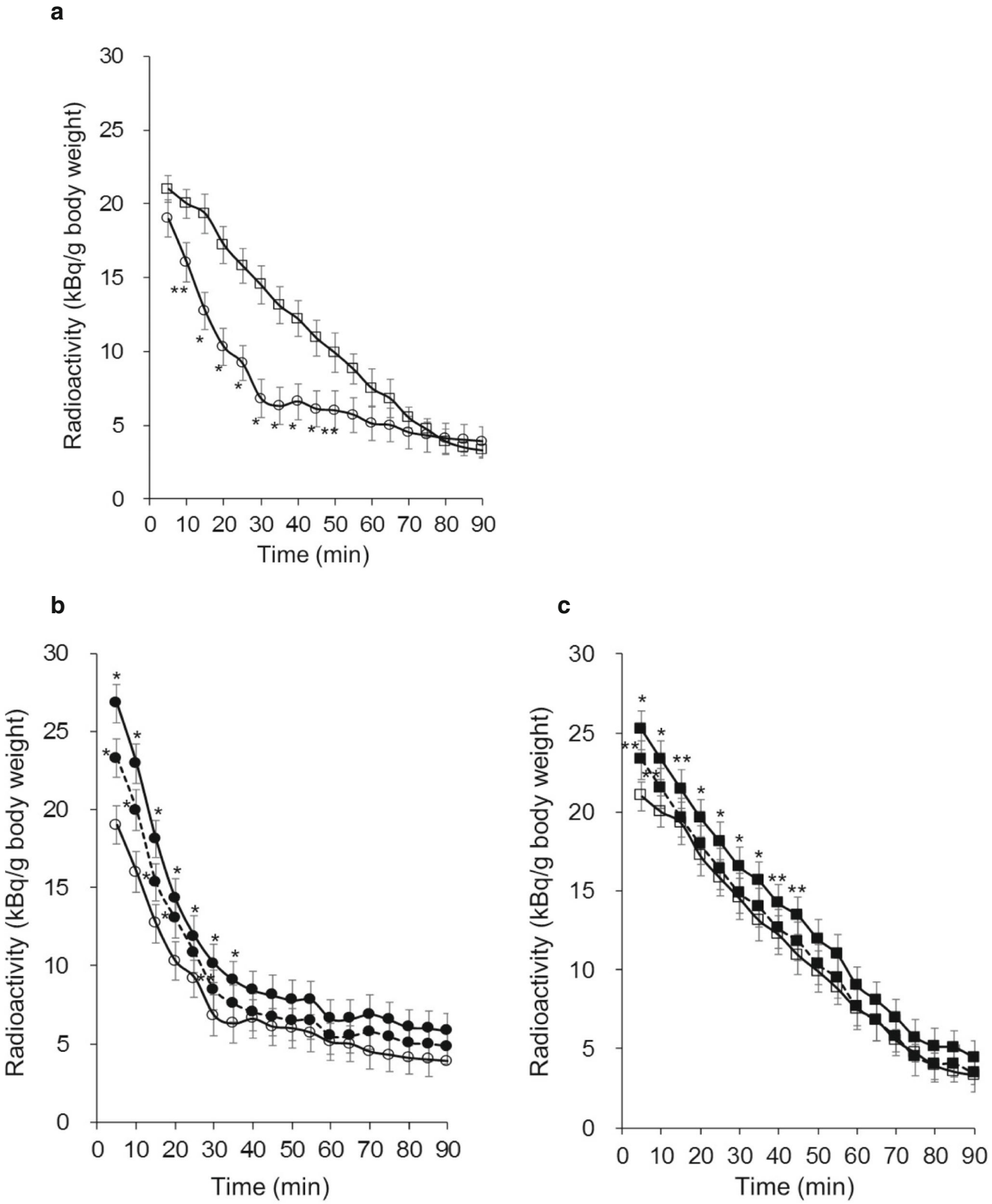

plasma, respectively, at 30 min after injection, and from 97.1 ± 4.0% to 35.7 ± 16.8%, 35.9 ± 16.8%, 85.1 ± 20.3%, and 72.4 ± 21.2% in SK-N-SH cells, mouse liver, human liver S9 fractions, and plasma, respectively, at 60 min after injection. On the other hand, ^{99m}Tc-TF was stable at about more than 95% at all injection times in all tissues.

Table II Metabolism Ratios of ^{99m}Tc-MIBI and ^{99m}Tc-TF in SK-N-SH Cells, Mouse Liver, Human Liver S9 Fractions, and Plasma

Time (min)	^{99m}Tc-MIBI (%)				^{99m}Tc-TF (%)			
	SK-N-SH	Mouse liver	Human liver S9	Plasma	SK-N-SH	Mouse liver	Human liver S9	Plasma
30	32.4 ± 17.5	26.3 ± 14.2	79.9 ± 18.5	62.9 ± 12.1	1.1 ± 0.2	1.3 ± 0.3	3.5 ± 0.7	1.8 ± 0.2
60	35.7 ± 16.8	35.9 ± 16.8	85.1 ± 20.3	72.4 ± 21.2	3.5 ± 1.3	4.0 ± 0.8	4.6 ± 0.9	4.3 ± 0.2

The fractional ratios of metabolites were calculated by dividing the radioactive counts for each fraction by the total radioactivity count

DISCUSSION

Although ^{99m}Tc-MIBI and ^{99m}Tc-TF are known to be exported via efflux transporters (6–12), several different kinds of efflux transporters have not been evaluated yet. In the vesicle assay, ^{99m}Tc-MIBI had affinity for MDR1 and MRP1, whereas ^{99m}Tc-TF showed affinity for not only MDR1 and MRP1 but also MRP2 and MRP3, as indicated by the significant difference in uptake between ATP and AMP loading, which shows the effect of each efflux transporter in the vesicle study (Fig. 1). In addition, uptake of the ^{99m}Tc-labeled compounds in vesicles was inhibited by verapamil for MDR1 and MK-571 for MRP. The data confirmed that ^{99m}Tc-MIBI and ^{99m}Tc-TF are exported via MDR1 (6–8) and MRP1 (7), and our data show that ^{99m}Tc-TF is also transported by MRP2 and MRP3.

To confirm the mechanism and the affinity of efflux of ^{99m}Tc-labeled compounds via the ABC transporters in human cancer cells, we selected SK-N-SH cells, which express MDR1 and MRP1, as model cancer cells that highly express ABC transporters. In the assay (Fig. 2), because uptake of ^{99m}Tc-labeled compounds was significantly increased by verapamil and MK-571 inhibitors, the efflux mechanism of ^{99m}Tc-labeled compounds could be identified as involving MDR1 and MRP1. The time activity curves of both ^{99m}Tc-labeled compounds and MK-571 loading showed significantly higher uptake than in the control condition or with verapamil loading, although MDR1 and MRP1 are expressed at similarly high levels in SK-N-SH cells. Thus, when MDR1 and MRP1 are highly expressed in cancers, ^{99m}Tc-labeled compounds will be exported via MDR1 and MRP1, but MRP1 is more sensitive than MDR1. Time activity curves of ^{99m}Tc-MIBI with each inhibitor showed higher uptake than that of ^{99m}Tc-TF with each inhibitor. Therefore, ^{99m}Tc-MIBI is exported via MDR1 and MRP1 (MDR1 < MRP1) at greater levels and more quickly than ^{99m}Tc-TF, and this is important for MDR monitoring. Although Gomes *et al.* have also reported that ^{99m}Tc-MIBI is more sensitive to MRP1 than ^{99m}Tc-TF *in vitro* (8), they evaluated the relationship between ^{99m}Tc-labeled compounds and efflux transporters using a small-cell lung cancer cell line with single overexpression of MDR1 or MRP1. Because cancer cells usually overexpress multiple transporters, e.g., MDR1 and/or MRP1–3, our results strongly certified that ^{99m}Tc-MIBI is more sensitive to MRP1 than ^{99m}Tc-TF using cancer cells that overexpress both MDR1 and MRP1.

Time activity curves of ^{99m}Tc-MIBI with MK-571 loading showed very little difference in accumulation in SK-MEL-28 and PC-3 cells (Fig. 3a). Regarding MDR expression in PC-3 and SK-MEL-28 cells (Table I), although little MDR1 expression was seen in either cell line, MRP1 expression in PC-3 cells was higher than that in SK-MEL-28 cells. When expression of MRP1 is somewhat high in cancer cells, time activity curves of ^{99m}Tc-MIBI, which is exported via MDR1 and MRP1, may be similar. In the time activity curves of ^{99m}Tc-TF (Fig. 3b), ^{99m}Tc-TF with MK-571 loading in SK-MEL-28 cells, which express MRP1 and MRP2, showed higher accumulation than that in PC-3 cells, which express MRP1 and MRP3. Although ^{99m}Tc-TF was exported by not only MDR1 and MRP1 but also MRP2 and MRP3, MRP3 may have a smaller effect than MRP1 and MRP2 in export of ^{99m}Tc-TF.

In whole-body imaging of a SK-N-SH-bearing mouse injected with ^{99m}Tc-MIBI (Fig. 4a) or ^{99m}Tc-TF (Fig. 4b) at 5–10 min (c, f), 30–35 min (d, g), and 55–60 min (e, h), accumulation in SK-N-SH cells was lower than in abdominal organs at all acquisition times. Although we observed similar accumulation levels between ^{99m}Tc-MIBI (Fig. 4Ac) and ^{99m}Tc-TF (Fig. 4Bf) at 5–10 min after injection in SK-N-SH cells, accumulation of ^{99m}Tc-MIBI in liver was lower than that of ^{99m}Tc-TF. Liver mainly expresses MDR1, MRP2, BCRP, and the bile salt export pump, which are ABC transporters that are the same types of MDR efflux transporters expressed in tumor cells. We suggest that ^{99m}Tc-MIBI is transferred quickly from liver to gallbladder after injection. At 30–35 min after injection, the accumulation of ^{99m}Tc-MIBI (Fig. 4Ad) was likely lower than that of ^{99m}Tc-TF (Fig. 4Bg) in SK-N-SH cells, and background levels of ^{99m}Tc-MIBI were also lower than those of ^{99m}Tc-TF because excretion of ^{99m}Tc-MIBI was faster than that of ^{99m}Tc-TF (Fig. 5).

The whole-body distribution of ^{99m}Tc-MIBI (Fig. 5a) and ^{99m}Tc-TF (Fig. 5b) was obtained from whole-body images. Because liver and kidney express MDR1 but not MRP1 for efflux and excretion of both ^{99m}Tc-labeled compounds (20), ^{99m}Tc-MIBI showed faster transport to the gallbladder and quicker excretion via MDR1 than ^{99m}Tc-TF. Therefore, we found that ^{99m}Tc-MIBI is sensitive to the ABC transporter, MDR1, in whole-body imaging. In the parathyroid and heart, accumulation did not change much over time, but ^{99m}Tc-MIBI

showed higher accumulation than ^{99m}Tc-TF because few ABC transporters are expressed in normal conditions in the parathyroid and heart. Vrachimis *et al.* showed similar results as ours in liver and heart (21). Additionally, initial uptake of ^{99m}Tc-MIBI may be increased compared with ^{99m}Tc-TF.

Time activity curves of SK-N-SH cells in SK-N-SH-bearing mice from whole-body images in Fig. 4 showed that more ^{99m}Tc-MIBI underwent efflux from the tumors than ^{99m}Tc-TF during the first 50 min after injection (Fig. 6A). Although Gomes *et al.* also showed that export of ^{99m}Tc-MIBI is faster than that of ^{99m}Tc-TF in an *in vitro* study (8), we confirmed this observation in an *in vivo* study. The time activity curve of ^{99m}Tc-MIBI shifted from fast export to slightly moderate export at about 30 min after injection because we estimate that about half of ^{99m}Tc-MIBI was metabolized in cancer cells and liver about 35 min after injection, and the metabolites of ^{99m}Tc-MIBI will undergo minimal efflux from the tumors via MDR1 and MRP1. MK-517 loading for MRP inhibition in SK-N-SH cells provided the highest significant accumulation at about 35 min, whereas verapamil loading also yielded significantly higher accumulation than the control condition at about 30 min (Fig. 6B). The results of our *in vivo* study emphasized that export of ^{99m}Tc-MIBI is more sensitive to MRP1 than MDR1, and the metabolites of ^{99m}Tc-MIBI will be minimally exported via MDR1 and MRP1. On the other hand, ^{99m}Tc-TF underwent gradual efflux from the tumors via MDR1 and MRP1 in SK-N-SH cells over time (Fig. 4A) because we estimate that ^{99m}Tc-TF was much more stable at all scanning times. In the time activity curves of ^{99m}Tc-TF (Fig. 6C), verapamil and MK-571 loading increased the accumulation compared to the control condition at 10 min and 50 min, respectively. This result shows that export of ^{99m}Tc-TF is also more sensitive to MRP1 than MDR1. However, the effect of both inhibitors was smaller than the effect on ^{99m}Tc-MIBI because involvement of ^{99m}Tc-TF with MDR1 and MRP1–3 may be smaller than that of ^{99m}Tc-MIBI.

In clinical settings, MDR in solid cancers has been evaluated by comparing washout rates between the early time phase (10–30 min) and the late time phase (2–3 h) after injection of ^{99m}Tc-labeled compounds (4,5). If ^{99m}Tc-labeled compounds are metabolized in cancers and the liver completely and immediately after injection, monitoring of MDR in cancers may be affected because metabolites of ^{99m}Tc-labeled compounds may not be taken up in cancers and undergo efflux through MDR1 and MRP. In our study, ^{99m}Tc-MIBI was metabolized about 32%, 26%, and 80% in SK-N-SH cells, mouse liver, and human liver S9 at 30 min and about 36%, 36%, and 85% at 60 min after injection (Table II), respectively. Perek and Le Jeune evaluated monoglutathionyl conjugation in glioma cells with high levels of glutathione for drug metabolism using both ^{99m}Tc compounds (22,23). They showed that ^{99m}Tc-MIBI was metabolized to about 90% at 30 min, whereas ^{99m}Tc-TF was metabolized to about 20% at 30 min. The amounts of metabolites of ^{99m}Tc-MIBI were similar to those of human liver S9, but higher than in SK-N-SH cells because SK-N-SH cells may have less drug metabolizing enzyme including glutathione S-transferase than glioma cells (23). On the other hand, little metabolism of ^{99m}Tc-TF occurs in all tissues. These results were different from Jeune's results because ^{99m}Tc-TF may not be susceptible to metabolism by glutathione S-transferase in mice, human liver, and SK-N-SH cells. Additionally, mouse and human liver may have lower expression levels of glutathione S-transferase than glioma cells. Therefore, metabolites of ^{99m}Tc-TF may not have been present in our study. However, the influence of these metabolites will be small because ^{99m}Tc-MIBI shows MDR in the early time phase before metabolism of ^{99m}Tc-MIBI occurs (Fig. 4a). On the other hand, ^{99m}Tc-TF imaging showed accurate MDR using two scans in the early time phase and late time phase because ^{99m}Tc-TF is stable (Table II).

CONCLUSION

The efflux mechanism and metabolism of ^{99m}Tc-labeled compounds differed in human cancer cells and SK-N-SH-bearing mice. When cancers express MDR1 and MRP1, ^{99m}Tc-MIBI is exported via MDR1 and MRP1 (MRP1 > MDR1) at greater levels and more quickly compared to ^{99m}Tc-TF. ^{99m}Tc-TF is exported by not only MDR1 and MRP1 but also MRP2 and MRP3, although MRP3 has a smaller influence than MRP1 and MRP2 (MRP1 > MDR1; MRP1, 2 > MRP3). Because ^{99m}Tc-MIBI is metabolized in human-derived cancers and human liver S9 fractions, clinical imaging to monitor MDR1 and MRP1 will be possible, and shorter SPECT examination times may be possible by switching to an earlier scan time (0.5–1 h etc.) for late phase imaging at 2–3 h after injection. ^{99m}Tc-TF has high stability and reflects the function of MDR1 and MRP1–3.

ACKNOWLEDGMENTS AND DISCLOSURES

The authors thank the staff of the School of Health Sciences, Kanazawa University for their technical support. This study was partly funded by Grants-in-Aid for Scientific Research from the Japan Society for the Promotion of Science (Nos. 25,293,260, 15 K09949, 15 K15452, and 16KK0020).

Publisher's Note

REFERENCES

1. Lockhart A, Tirona L, Kim R. Pharmacogenetics of ATP-binding cassette transporters in cancer and chemotherapy. Mol Cancer Ther. 2003;2:685–98.
2. Kailasnath P, Sinusas AJ. Technetium-99m-labeled myocardial perfusion agents: are they better than thallium-201? Cardiol Rev. 2001;9(3):160–72.
3. Schillaci O, Spanu A, Madeddu G. [^{99m}Tc]sestamibi and [^{99m}Tc]tetrofosmin in oncology: SPECT and fusion imaging in lung cancer, malignant lymphomas and brain tumors. Q J Nucl Med Mol Imaging. 2005;49(2):133–44.
4. Kostakoglu L, Kiratli P, Ruacan S, Hayran M, Emri S, Ergün EL, et al. Association of tumor washout rates and accumulation of technetium-99m-MIBI with expression of P-glycoprotein in lung cancer. J Nucl Med. 1998;39:228–34.
5. Kurata S, Ushijima K, Kawahara A, Kaida H, Kawano K, Hirose Y, et al. Assessment of 99mTc-MIBI SPECT(/CT) to monitor multidrug resistance-related proteins and apoptosis-related proteins in patients with ovarian cancer: a preliminary study. Ann Nucl Med. 2015;29:643–9.
6. Piwnica-Worms D, Chiu ML, Budding M, Kronauge JF, Kramer RA, Croop JM. Functional imaging of multidrug-resistant P-glycoprotein with an organotechnetium complex. Cancer Res. 1993;53:977–84.
7. Kinuya S, Li XF, Yokoyama K, Mori H, Shiba K, Watanabe N, et al. Reduction of ^{99m}Tc-sestamibi and ^{99m}Tc-tetrofosmin uptake in MRP-expressing breast cancer cells under hypoxic conditions is independent of MRP function. Eur J Nucl Med Mol Imaging. 2003;30:1529–31.
8. Gomes CM, Abrunhosa AJ, Pauwels EK, Botelho MF. P-glycoprotein versus MRP1 on transport kinetics of cationic lipophilic substrates: a comparative study using [^{99m}Tc]sestamibi and [^{99m}Tc]tetrofosmin. Cancer Biother Radiopharm. 2009;24:215–27.
9. Yamasaki M, Makino T, Masuzawa T, Kurokawa Y, Miyata H, Takiguchi S, et al. Role of multidrug resistance protein 2 (MRP2) in chemoresistance and clinical outcome in oesophageal squamous cell carcinoma. Br J Cancer. 2011;104:707–13.
10. O'Brien C, Cavet G, Pandita A, Hu X, Haydu L, Mohan S, et al. Functional genomics identifies ABCC3 as a mediator of taxane resistance in HER2-amplified breast cancer. Cancer Res. 2008;68:5380–9.
11. Montani M, Hermanns T, Müntener M, Wild P, Sulser T, Kristiansen G. Multidrug resistance protein 4 (MRP4) expression in prostate cancer is associated with androgen signaling and decreases with tumor progression. Virchows Arch. 2013;462:437–43.
12. Nakanishi T, Ross DD. Breast cancer resistance protein (BCRP/ABCG2): its role in multidrug resistance and regulation of its gene expression. Chin J Cancer. 2012;31:73–99.
13. Kobayashi M, Nakanishi T, Nishi K, Higaki Y, Okudaira H, Ono M, et al. Transport mechanism of hepatic uptake and bile excretion in clinical hepatobiliary scintigraphy with ^{99m}Tc-N-pyridoxyl-5-methyltryptophan. Nucl Med Biol. 2014;41:338–42.
14. Kobayashi M, Hashimoto F, Ohe K, Nadamura T, Nishi K, Shikano N, et al. Transport mechanism of ^{11}C-labeled L- and D-methionine in human-derived tumor cells. Nucl Med Biol. 2012;39:1213–8.
15. Mohamed LA, Kaddoumi A. In vitro investigation of amyloid-β hepatobiliary disposition in sandwich-cultured primary rat hepatocytes. Drug Metab Dispos. 2013;41:1787–96.
16. Sakamoto S, Suzuki H, Kusuhara H, Sugiyama Y. Efflux mechanism of taurocholate across the rat intestinal basolateral membrane. Mol Pharm. 2006;3:275–81.
17. Reed JR, Backes WL. Formation of P450. P450 complexes and their effect on P450 function. Pharmacol Ther. 2012;133:299–310.
18. Japan Radiopharmaceuticals Association: The Minimum Requirements for Radiopharmaceuticals. http://www.houyakkyou.org/img/housha_img/kaisetsu_160630.pdf. Accessed 5 Aug 2018.
19. Métayé T, Desmarquet M, Rosenberg T, Guilhot J, Bouin-Pineau MH. Rapid quality control for testing the radiochemical purity of 99Tc(m)-tetrofosmin. Nucl Med Commun. 2001;22:1139–44.
20. Shitara Y, Sato H, Sugiyama Y. Evaluation of drug-drug interaction in the hepatobiliary and renal transport of drugs. Annu Rev Pharmacol Toxicol. 2005;45:689–723.
21. Vrachimis A, Hermann S, Máthé D, Schober O, Schäfers M. Systematic evaluation of ^{99m}Tc-tetrofosmin versus ^{99m}Tc-sestamibi to study murine myocardial perfusion in small animal SPECT/CT. EJNMMI Res. 2012;2:21.
22. Perek N, Prevot N, Koumanov F, Frere D, Sabido O, Beauchesne P, et al. Involvement of the glutathione S-conjugate compounds and the MRP protein in Tc-99m-tetrofosmin and Tc-99m-sestamibi uptake in glioma cell lines. Nucl Med Biol. 2000;27(3):299–307.
23. Le Jeune N, Perek N, Denoyer D, Dubois F. Study of monoglutathionyl conjugates TC-99M-sestamibi and TC-99M-tetrofosmin transport mediated by the multidrug resistance-associated protein isoform 1 in glioma cells. Cancer Biother Radiopharm. 2005;20(3):249–59.